Supporting Information

Light-Soaking in Large Area Perovskite Solar Cells Driven by the Formation of Fullerene/BCP Charge Transfer Complexes

Charlie Henderson,[a] Joel Luke,[a] Izabela S. Bicalho,[b] Luiza Correa,[b] Emily J. Yang,[a] Martina Rimmele,[c] Harry Demetriou,[d] Yi-Chun Chin,[a] Tianhao Lan,[a] Sandrine Heutz,[d] Nicola Gasparini,[c] Martin Heeney,[c,e] Diego Bagnis[b] & Ji-Seon Kim*[a]

[a] Department of Physics and Centre for Processable Electronics, Imperial College London, London SW7 2AZ, UK

Email: ji-seon.kim@imperial.ac.uk

[b] Oninn, Av. José Cândido da Silveira 2000 - Horto Florestal, Belo Horizonte, MG31035-536, Brazil

[c] Department of Chemistry and Centre for Processable Electronics, Imperial College London, London W12 0BZ, UK

[d] Department of Materials and Centre for Processable Electronics, Imperial College London, London SW7 2AZ, UK

[e] KAUST Solar Center, Physical Science and Engineering Division, King Abdullah University of Science and Technology (KAUST), Thuwal, 23955-6900 Saudi Arabia

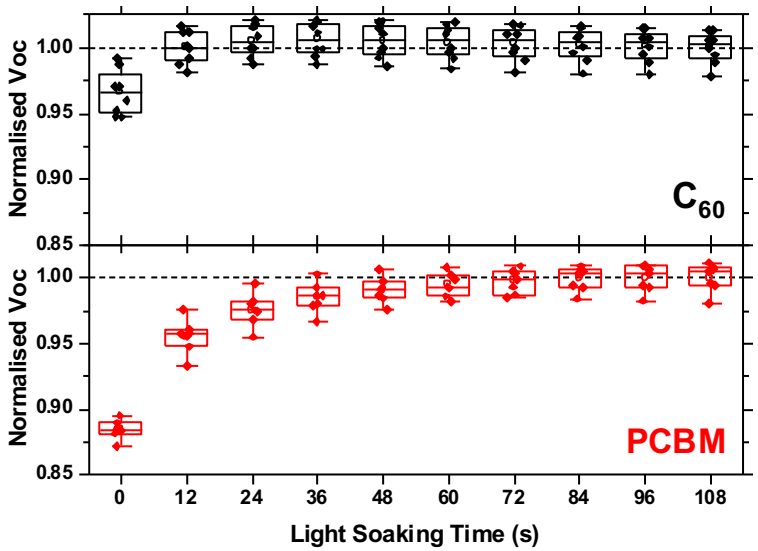

Figure S1: Change in V_{OC} over time for ITO/NiO/$MAPbI_3$/Fullerene/BCP/Ag devices under 1 Sun Illumination.

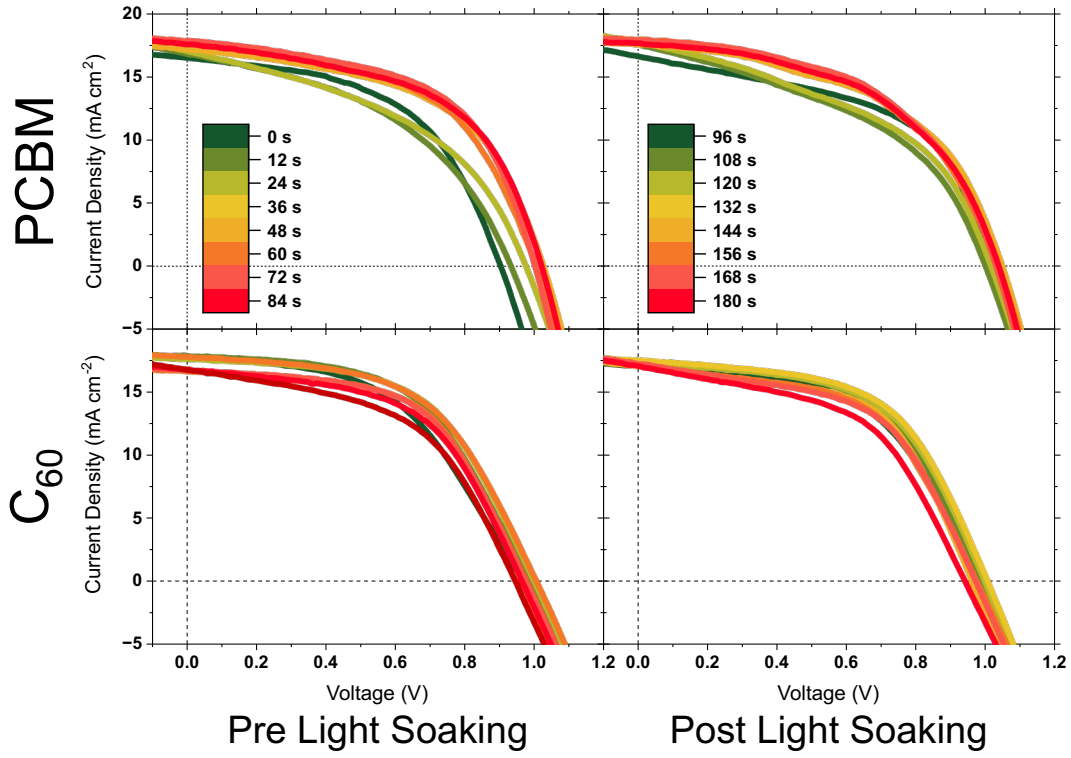

Figure S2: 1 Sun J/V characteristics of ITO/NiO/$MAPbI_3$/Fullerene/BCP/Ag devices before and after light soaking. Each device was comprised of 8 pixels which were scanned sequentially such that in the pre light soaking scans 'Pixel 8' had been exposed to illumination for ~80 s before measurement. Legend shows the time under illumination prior to testing for each measurement.

		V_{OC} (V)	J_{SC} (mA cm^{-2})	FF	PCE (%)
$PC_{61}BM$	**Pre LS**	1.00	16.58	0.581	9.62
	Post LS	1.08 (1.09±0.01)	16.85 (17.37±0.37)	0.572 (0.572+0.028)	10.44 (10.25±0.39)
C_{60}	**Pre LS**	1.02	18.40	0.522	9.84
	Post LS	1.03 (0.98±0.01)	17.67 (17.21±0.17)	0.539 (0.550±0.012)	9.81 (9.30±0.34)

Table S1: Performance parameters of representative ITO/NiO/$MAPbI_3$/Fullerene/BCP/Ag PSCs before and after light soaking for ~100 s. Given in parentheses are the average values of the performance parameters of ≥8 pixels, with standard deviations, after LS.

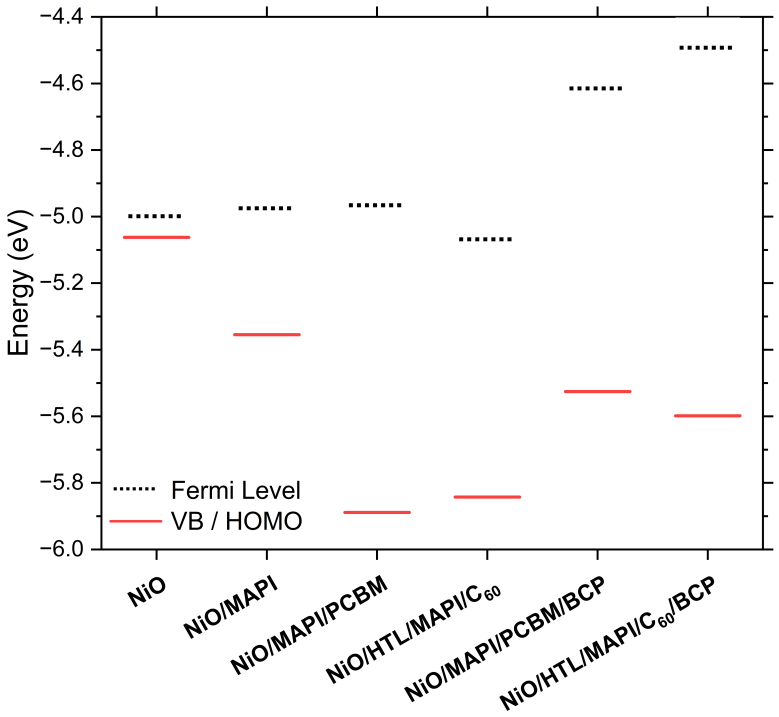

Figure S3**:** Results of energetic measurements of partial device stacks – both E_F and VB/HOMO level measurements are highly surface sensitive so the values are most influenced by the final layer. E_F measurements were taken prior to SPV and VB/HOMO level measurements were taken following SPV acquisition.

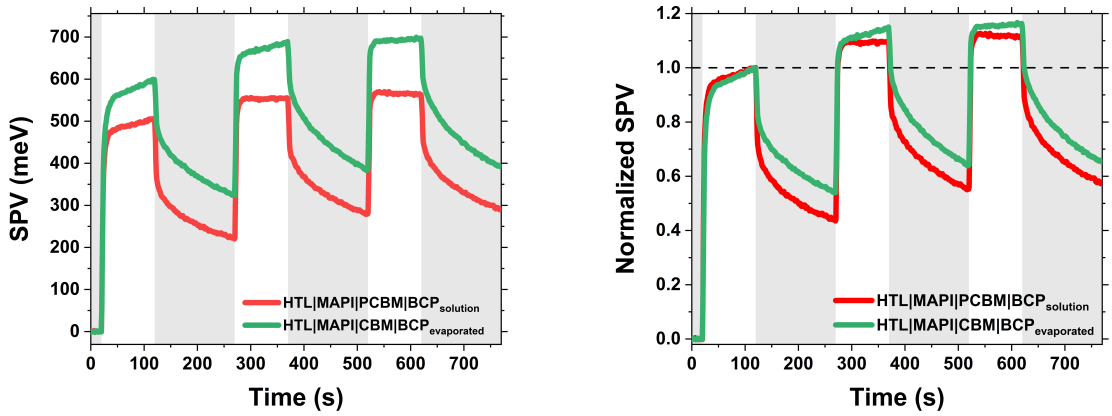

Figure S4: Raw and normalised transient SPV responses of ITO/NiO/$MAPbI_3$/PCBM/BCP samples with 10 nm thick solution processed BCP (red) and 5 nm thick evaporated BCP (green).

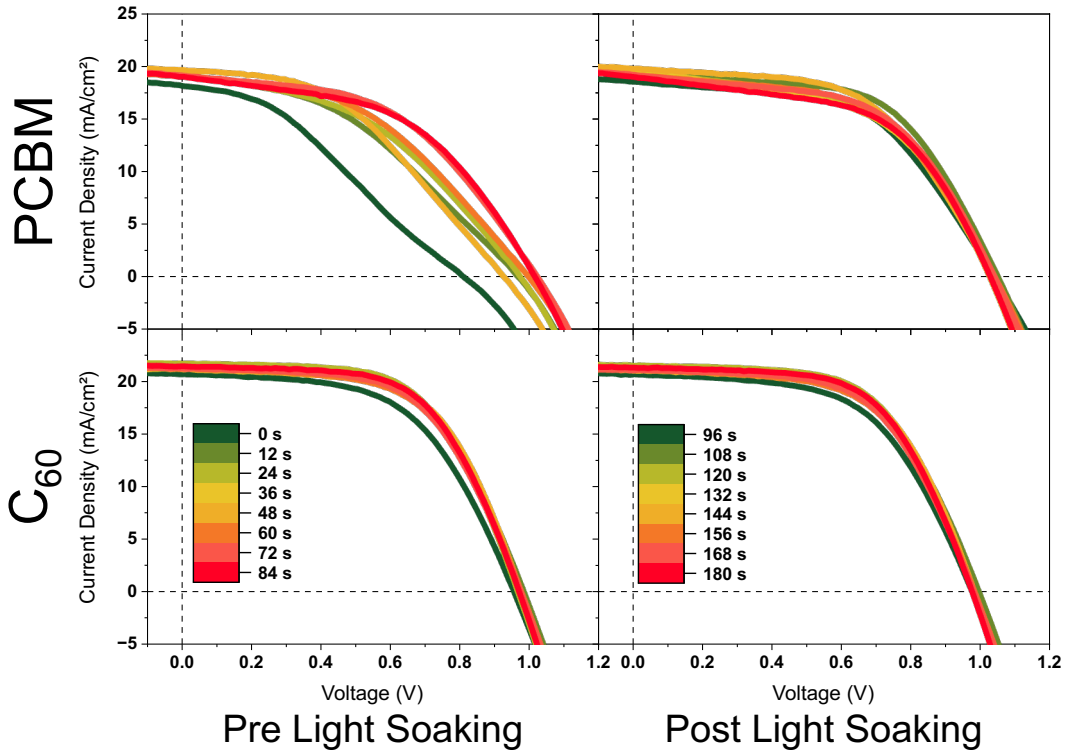

Figure S5: 1 Sun J/V characteristics of ITO/NiO/$Cs_xFA_{1-x}PbI_3$/Fullerene/BCP/Ag devices before and after light soaking. Each device was comprised of 8 pixels which were scanned sequentially such that in the pre light soaking scans 'Pixel 8' had been exposed to illumination for ~80 s before measurement. Legend shows the time under illumination prior to testing for each measurement.

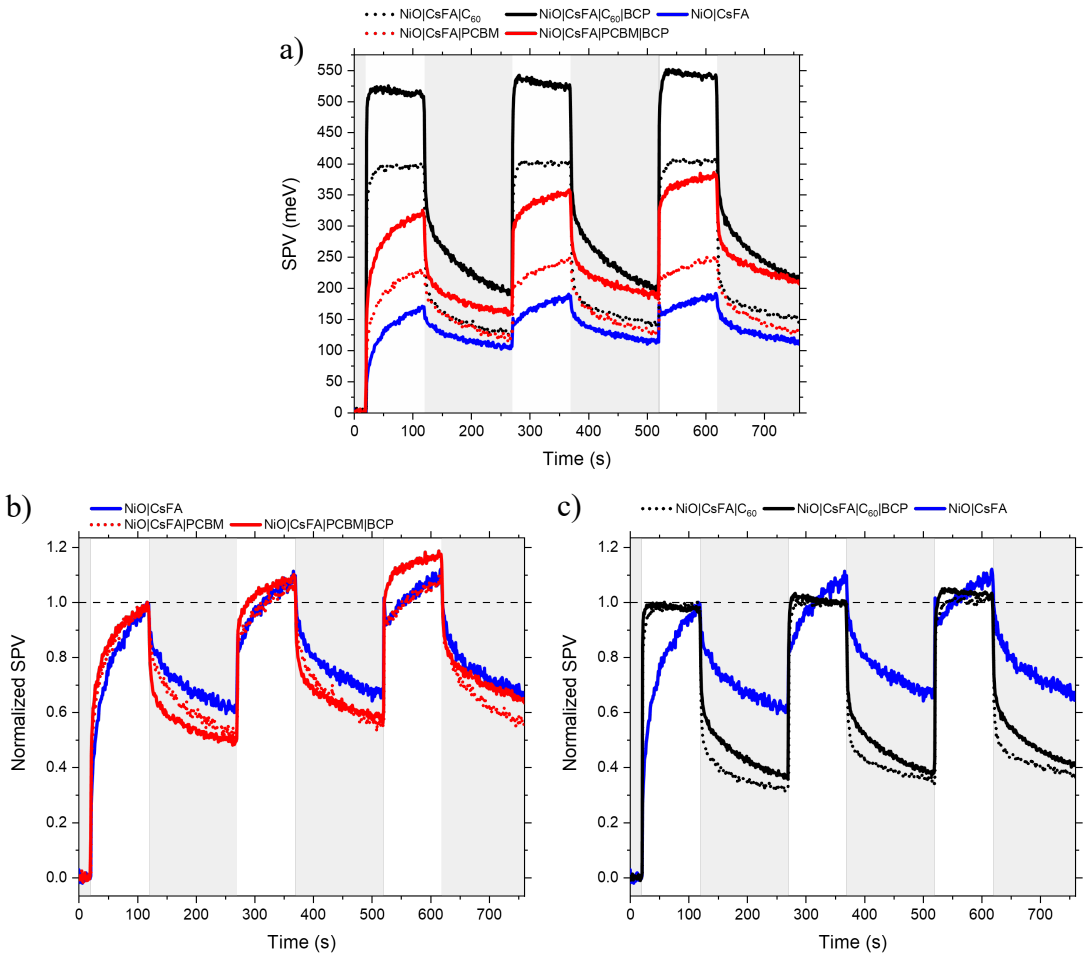

Figure S6: Raw (a) and normalised (b,c) SPV responses of samples with the same structures as in Figure 2, utilising an $Cs_xFA_{1-x}PbI_3$ photoactive layer in place of $MAPbI_3$.

Discussion of $Cs_xFA_{1-x}PbI_3$ SPV: Interpretation of the SPV response of the $Cs_xFA_{1-x}PbI_3$ perovskite is complicated by the slow turn on characteristics intrinsic to this particular perovskite (detailed on page 9 of the main text). This effect is very significant in the $Cs_xFA_{1-x}PbI_3$, $Cs_xFA_{1-x}PbI_3$/PCBM, and $Cs_xFA_{1-x}PbI_3$/PCBM/BCP samples when compared to their MAPI counterparts (Fig. 2). The origin of this is unclear but is possibly related to the multi-cation composition of the perovskite resulting in changes to the surface chemistry. At short times (i.e. during the first cycle) the effect of the BCP LS effect is masked by the changes at the $Cs_xFA_{1-x}PbI_3$/PCBM interface. Figure S6b shows the SPV response normalised to the SPV signal at the end of the first cycle (t= 120 s). We interpret the increased relative SPV signal from the PCBM/BCP sample in the second and third cycles as evidence for light induced interaction between PCBM and BCP becoming resolvable from the perovskite induced slow process.

To further quantify these changes, we have fitted the slow turn-ons of the $Cs_xFA_{1-x}PbI_3$/PCBM based perovskite samples using a bi-exponential growth equation (Equation S1) where τ is the exponential lifetime, t is time in seconds after time = 0 (t_0), A is the pre-exponential factor and SPV is the SPV intensity in meV.

$$SPV(t) = SPV_0 + A_1 e^{-(t-t0)/\tau 1} + A_2 e^{-(t-t0)/\tau 2} \quad \text{(Equation S1)}$$

The results of these fittings for the first illumination cycle are shown below. As can be seen the introduction of BCP onto the $Cs_xFA_{1-x}PbI_3$/PCBM sample results in an increase in both the t_1 and t_2 lifetimes.

The intrinsic differences between the two perovskite compositions used in this study make direct comparison of the SPV results complex. However, the data presented in Figures 2, S6 and S7 supports the primary finding of the SPV portion of the study – that addition of the BCP layer to the PCBM samples introduces an additional slow process which slows the growth of the SPV magnitude.

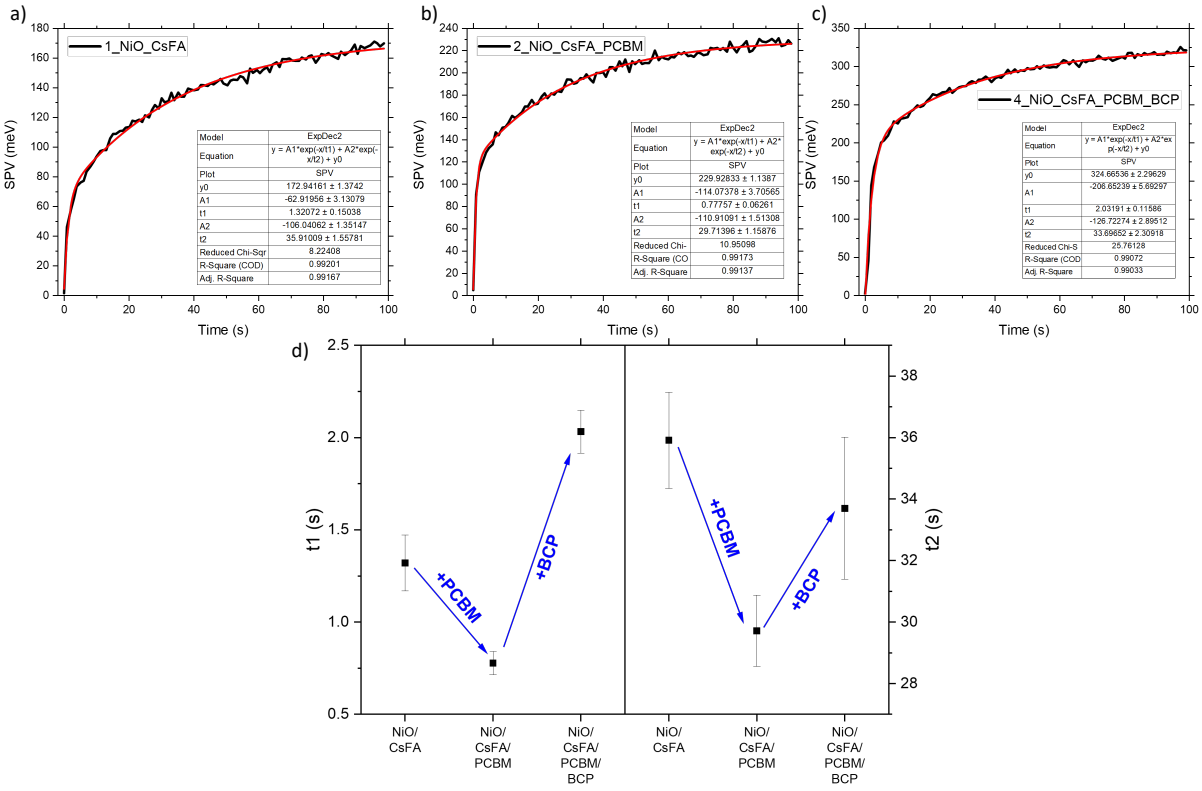

Figure S7: Fitted first cycle SPV responses, shown in Fig. S6, of a) ITO/NiO/$Cs_xFA_{1-x}PbI_3$, b) ITO/NiO/$Cs_xFA_{1-x}PbI_3$/PCBM, and c) ITO/NiO/$Cs_xFA_{1-x}PbI_3$/PCBM/BCP samples. d) shows the extracted t_1 and t_2 lifetimes of each sample.

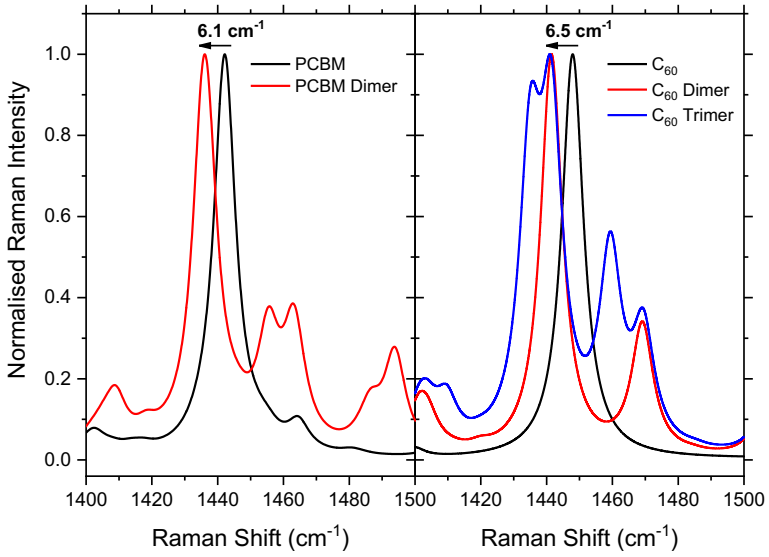

Figure S8: Simulated Raman spectra of PCBM (left) and C_{60} (right) molecules (black lines), dimers (red lines) and C_{60} trimers (blue line). Simulations carried out using DFT after molecular geometry optimisation.

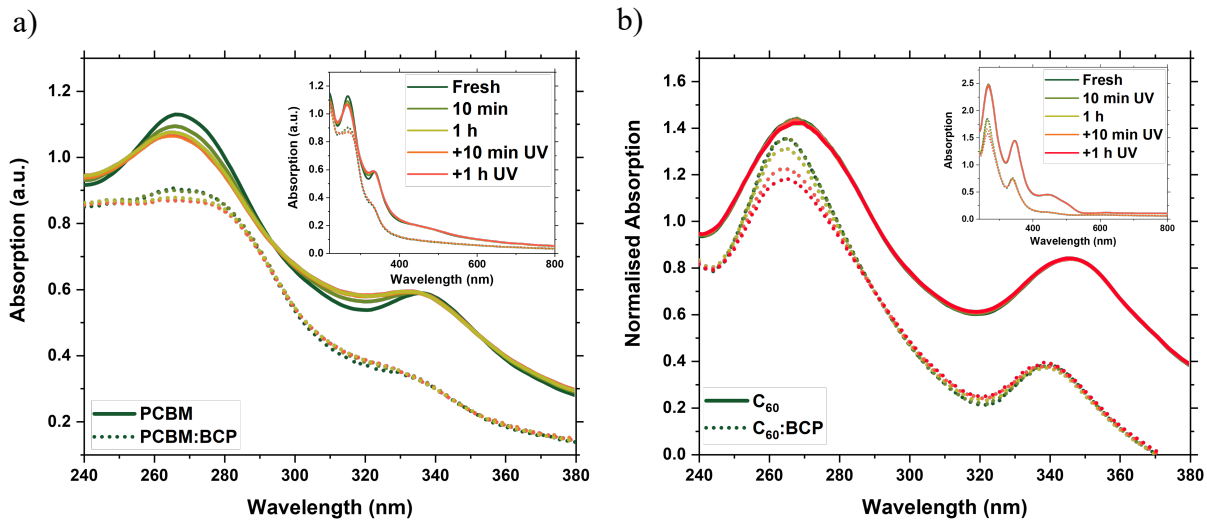

Figure S9: Absorption Spectra of neat fullerene (solid lines) and fullerene/BCP blend films (dashed lines) of a) PCBM and b) C_{60} during 1 Sun and 365 nm accelerated aging.

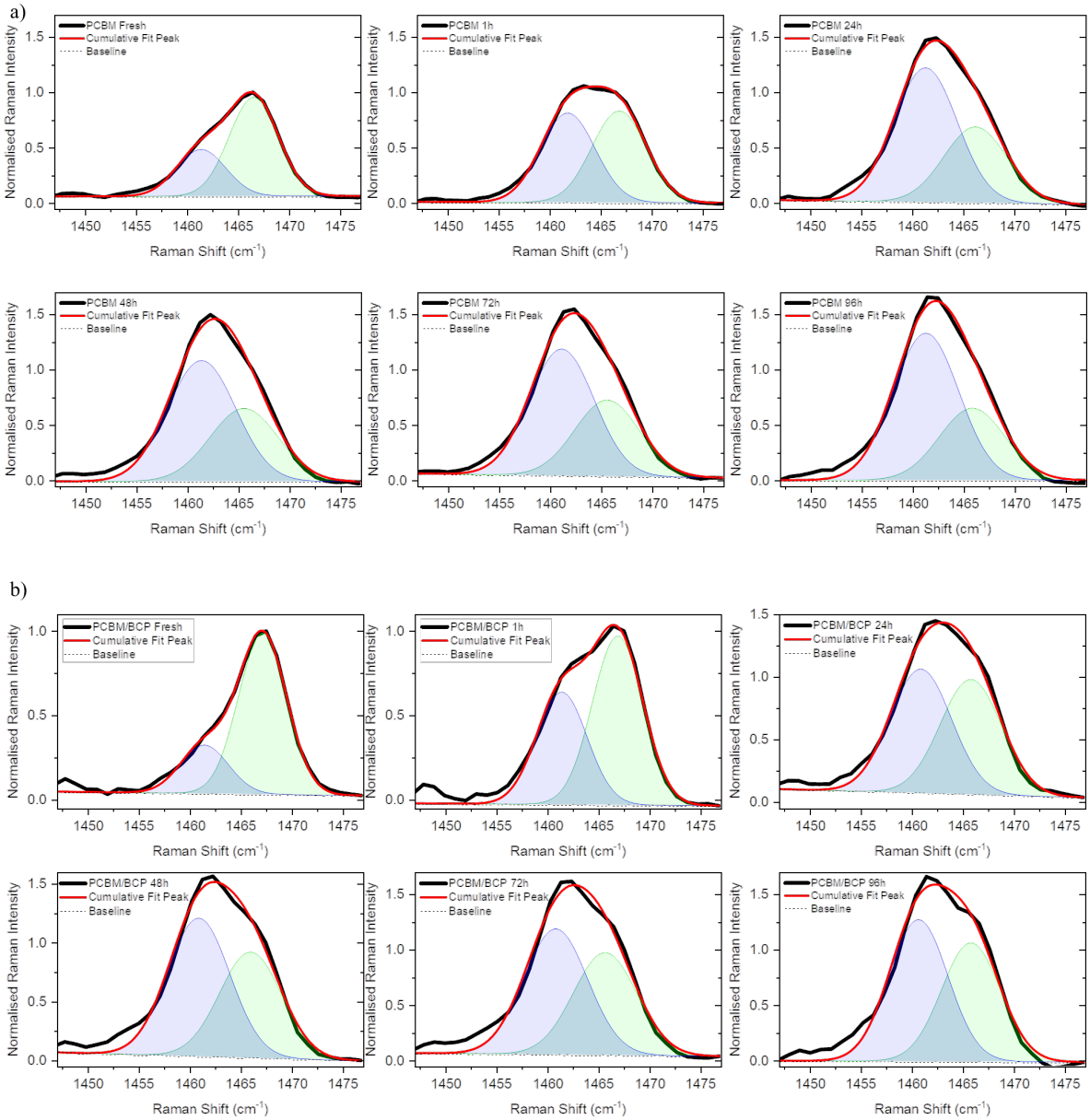
a)
PCBM Fresh
PCBM 1h
PCBM 24h
PCBM 48h
PCBM 72h
PCBM 96h
Cumulative Fit Peak
Baseline
Normalised Raman Intensity
Raman Shift (cm-1)
b)
PCBM/BCP Fresh
PCBM/BCP 1h
PCBM/BCP 24h
PCBM/BCP 48h
PCBM/BCP 72h
PCBM/BCP 96h

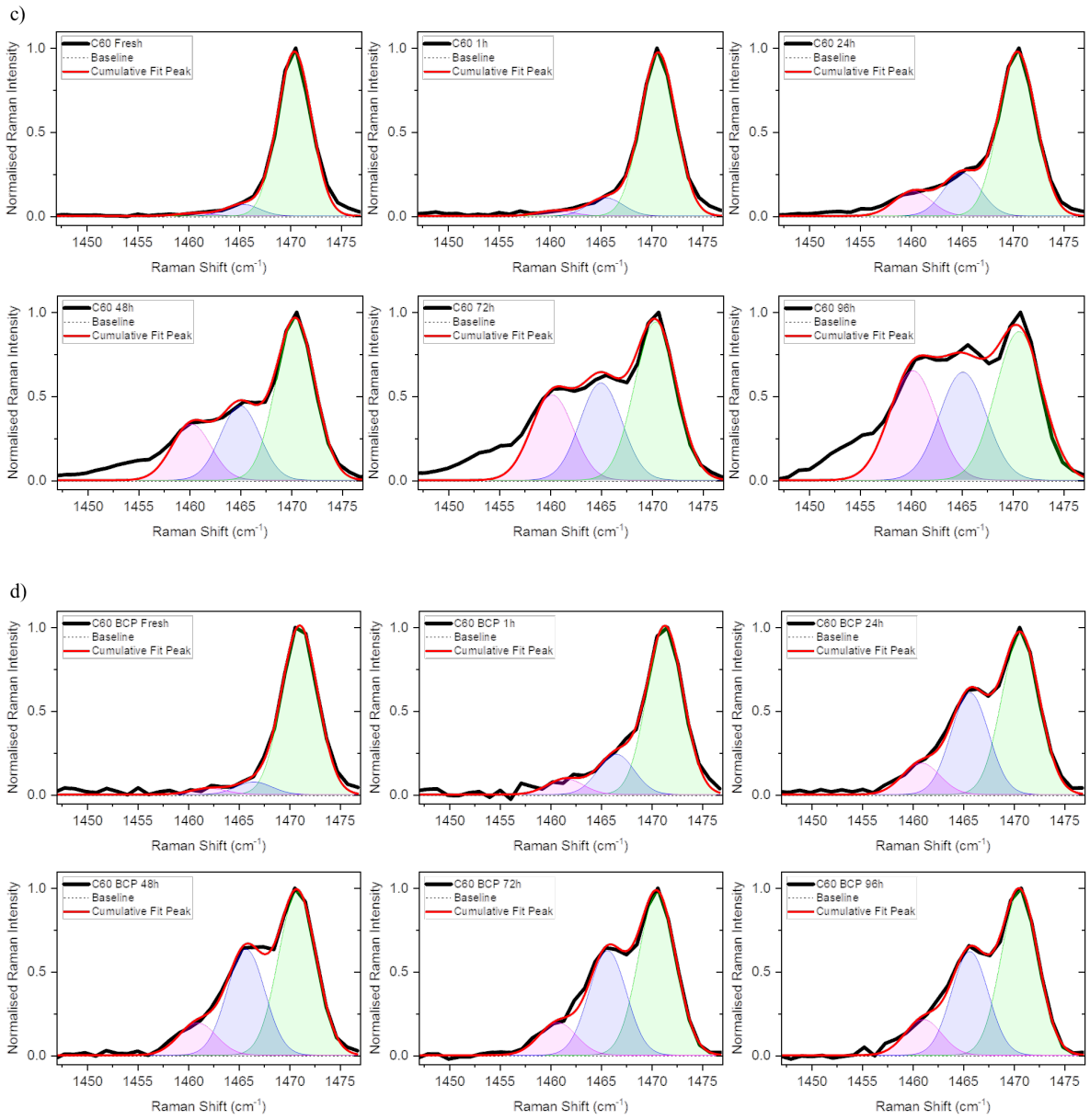

Figure S10: Deconvoluted Gaussian peak fittings of the Raman spectra shown inFigure S3 for a) PCBM, b) PCBM/BCP, c) C_{60} and d) C_{60}/BCP films. Green peaks are assigned to the A_g Raman modes of PCBM/C_{60} molecules, blue peaks to dimers and pink peaks to C_{60} trimers. Raman spectra are normalised to the intensity of the higher energy, monomer peak.

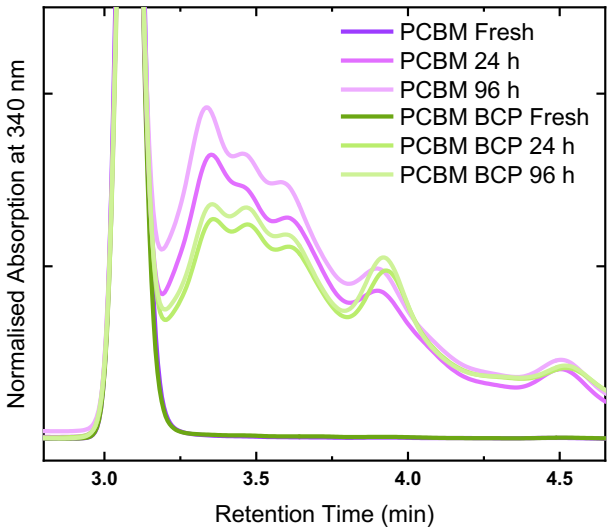

Figure S11: HPLC analyses normalised to the monomer signal at 340 nm of re-dissolved PCBM and PCBM/BCP films aged in 1 Sun conditions under an N_2 atmosphere.

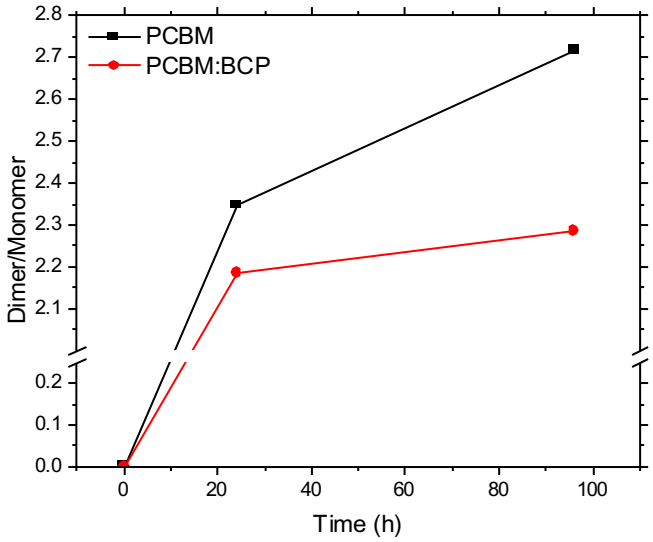

Figure S12: Dimer/Monomer peak area ratios extracted by integrating the respective areas of the HPLC analyses shown in Fig. S11.

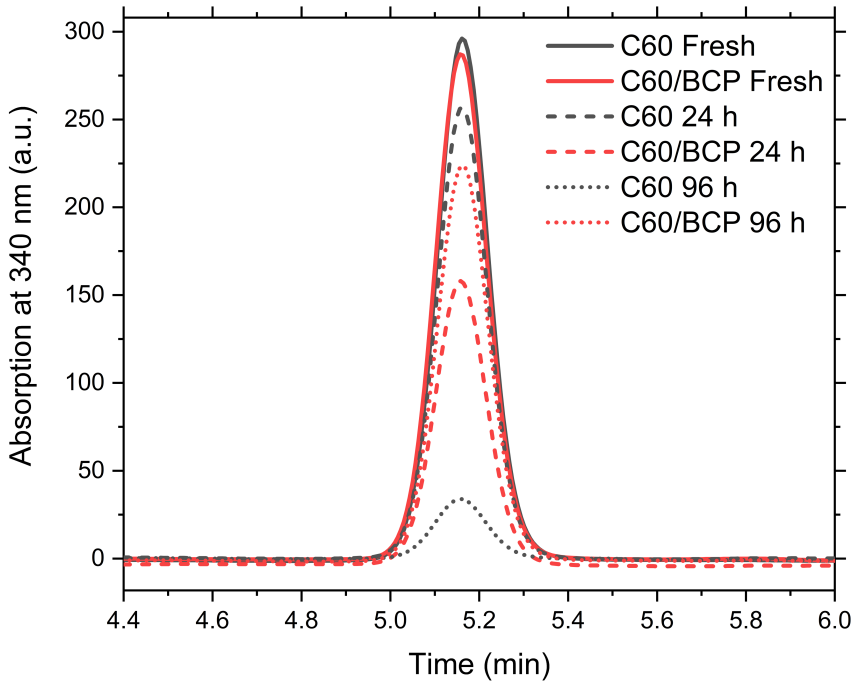

Figure S13: HPLC analyses of dissolved C_{60} and C_{60}/BCP films aged in 1 Sun conditions under an N_2 atmosphere.

***Discussion of HPLC Analyses*:** PCBM/PCBM dimers appear in the light soaked PCBM films as additional absorption peaks at longer retention times than the main PCBM peak (Fig. S11).[1] The occurrence of a broad signal for the dimers can be attributed to the formation of different regioisomers, which leads to differences in retention time.[1,2] HPLC analysis was also carried out on dissolved C_{60} and C_{60}:BCP films, with the analyses shown in Figure S10. No evidence of dimer or oligomer formation is observed, however this may be due to the poor solubility of C_{60} leaving the concentration of dimers below the limit-of-detection of the instrument. This is supported by the intensity of the main fullerene absorption peak in the fresh C_{60} analyses being ~10% of the peak in the PCBM analyses. When comparing the intensities of the absorption peaks of the HPLC analyses of the C_{60} and C_{60}:BCP films a clear decrease is observed in peak intensity upon LS, suggesting that molecular C_{60} is becoming less concentrated in the analyte solution. This effect is more pronounced in the neat C_{60} samples than in the C_{60}:BCP blend, with the 96 h light soaked C_{60} peak dropping to 11% of the intensity of the fresh C_{60} peak. As already discussed, the C_{60} films (particularly those which had undergone aging) exhibited poor solubility. This hindered further interpretation of the HPLC analyses due to the difficulty deconvoluting the contributions of products and contaminants.

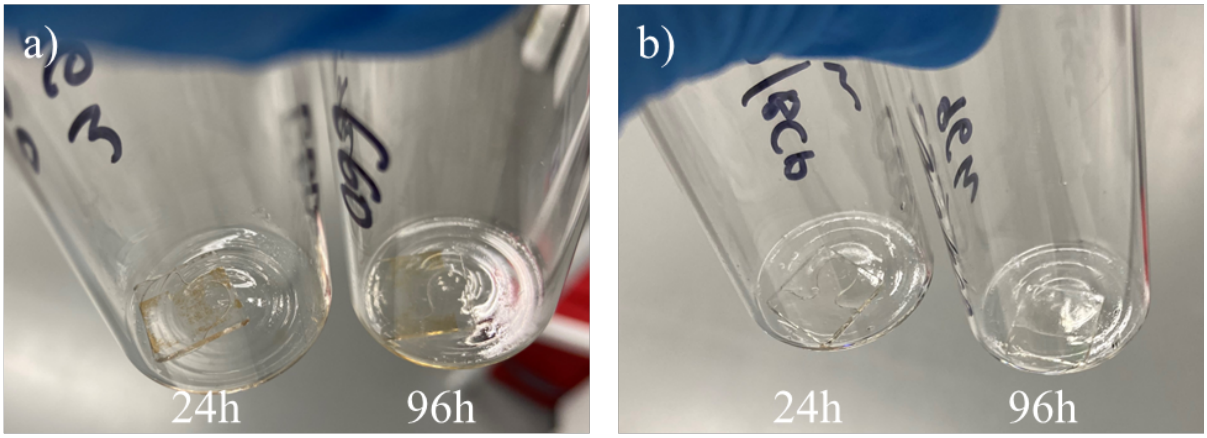

Figure S14: Photographs showing 24h (left) and 96h (right) a) C_{60} and b) C_{60}/BCP films following submersion in toluene.

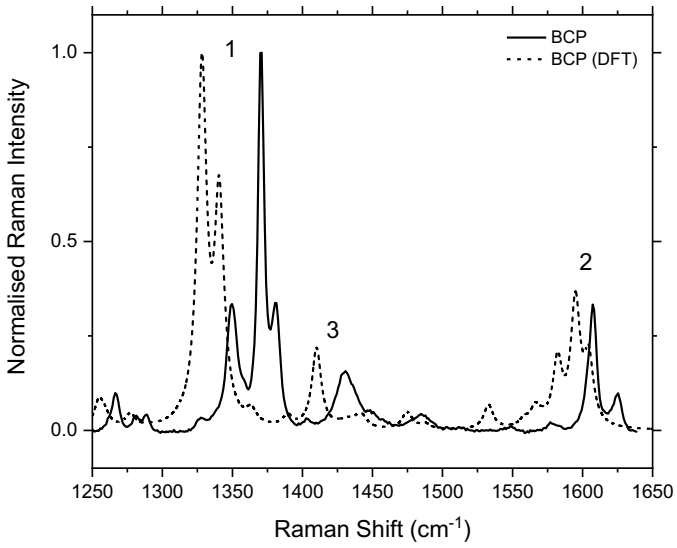

Figure S15: Experimental (solid line) and simulated (dashed line) Raman spectra of BCP.

Peak	Experimental Raman Shift (cm^{-1})	Simulated Raman Shift (cm^{-1})	Assignment
1	1370	1328	Phenanthroline a_1 (intra pyridine ring C-C stretch)
2	1607	1595	Phenyl e_{2g} (intra ring C-C stretch)
3	1430	1409	Phenanthroline b_1 (inter pyridine ring C-C stretch)

Table S2: Raman peak shifts and assignments for the spectra shown in S15, assignments for phenanthroline modes made with the assistance of Reiher et al.[3]

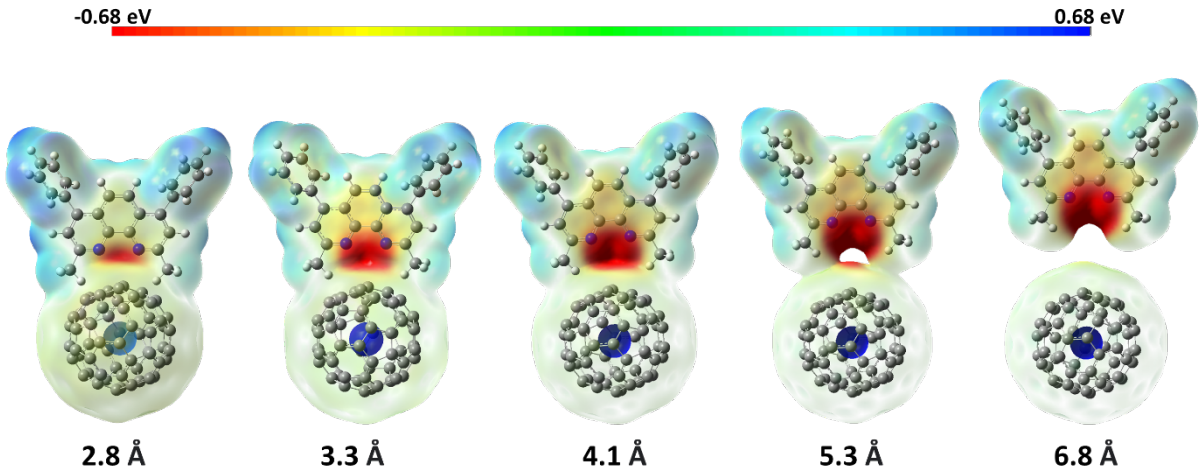

Figure S16: Electrostatic potential (ESP) maps of BCP and C_{60} molecules at increasing intermolecular distances. The distance given below each map refers to the distance between the closest BCP nitrogen and C_{60} carbon atoms. ESP calculates the energy of the repulsive (positive) or attractive (negative) force experienced by a positive point charge in close proximity to the molecule. Note the change in potential over the whole C_{60} molecule as the intermolecular spacing decreases, indicating increased electron density on the C_{60} at small spacings.

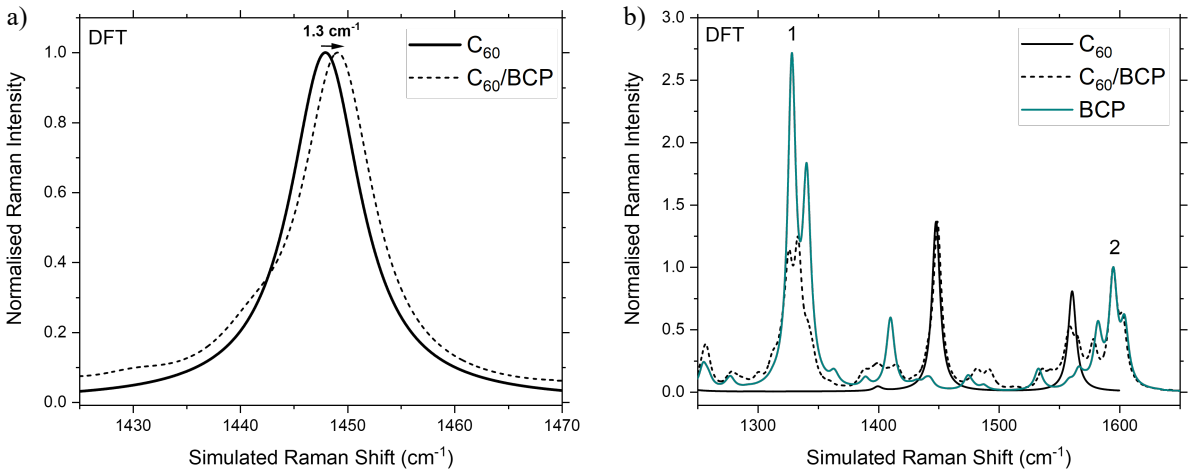

Figure S17: Simulated Raman spectra of C_{60}, BCP, and the 2.8 Å spacing C_{60}/BCP CT complex shown in Figure S15. a) 50 cm^{-1} wide region of the spectra showing the fullerene peaks only, b) 400 cm^{-1} wide region showing the fullerene and BCP peaks (normalised to 'Peak 2').

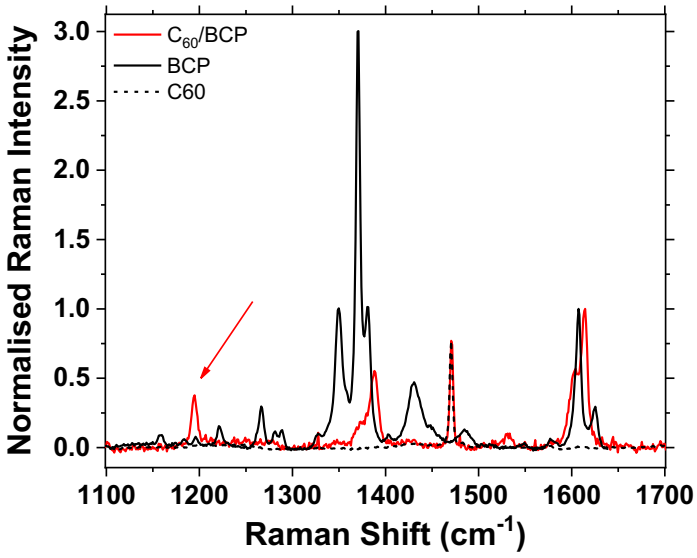

Figure S18: Raman spectra of fresh BCP (black), C_{60}/BCP blend (red) and C_{60} (black dashed) films. Upon aging under 1 Sun conditions no changes in the shift, FWHM or relative intensity of the peak at 1195 cm^{-1} are observed.

***Discussion of Possible BCP/C_{60} Adduct Formation*:** The appearance of a new Raman peak at 1195 cm^{-1} (the C-N bond region)[4] suggests that an adduct of C_{60} and BCP may be forming spontaneously in the blend (Fig. S17). We have previously reported spontaneous C_{60} adduct formation with a planar acceptor molecule (MPTA) containing a tertiary pyrrole nitrogen.[5] However, increased relative intensity of a small BCP peak in the same position cannot be ruled out, therefore, on balance, non-covalent CT complex formation is a more likely cause.

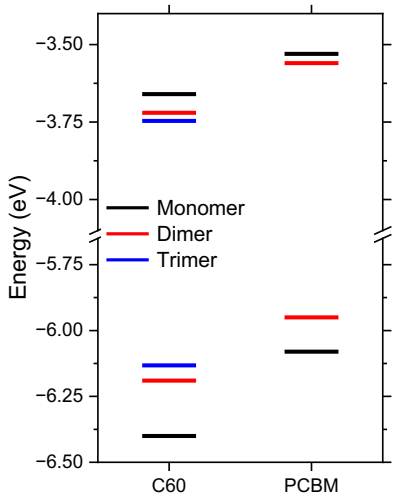

Figure S19: Simulated frontier molecular orbital energies of C_{60} (left) and PCBM (right) monomers (black), dimers (red) and trimers (blue). Simulations carried out using DFT after molecular geometry optimisation.

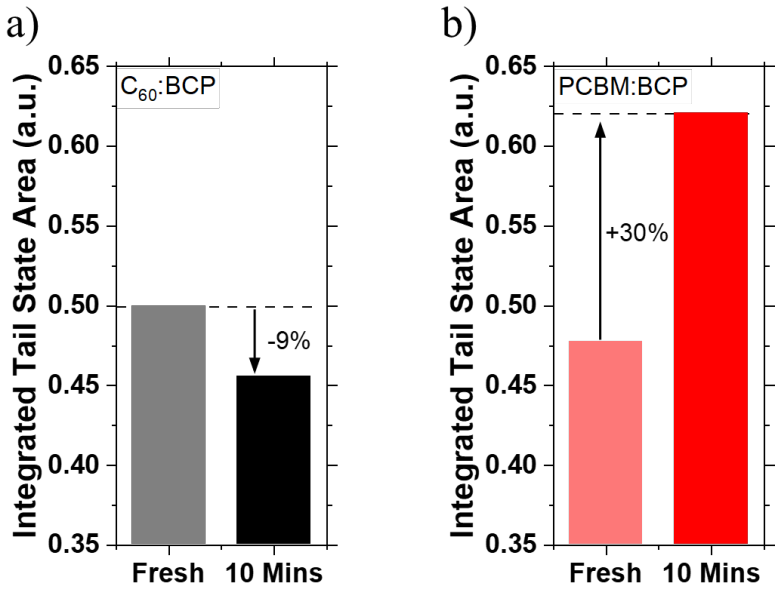

Figure S20: Integrated tail state areas before and after 10 mins LS of APS spectra shown in Figures 5a, 5b. a) C_{60}:BCP and b) $PC_{61}BM$:BCP.

References

1 T. Heumueller, W. R. Mateker, A. Distler, U. F. Fritze, R. Cheacharoen, W. H. Nguyen, M. Biele, M. Salvador, M. von Delius, H.-J. Egelhaaf, M. D. McGehee and C. J. Brabec, *Energy Environ. Sci.*, 2016, **9**, 247–256.

2 A. Distler, T. Sauermann, H.-J. Egelhaaf, S. Rodman, D. Waller, K.-S. Cheon, M. Lee and D. M. Guldi, *Adv. Energy Mater.*, 2014, **4**, 1300693.

3 M. Reiher, G. Brehm and S. Schneider, *J. Phys. Chem. A*, 2004, **108**, 734–742.

4 J. E. Stewart, *J. Chem. Phys.*, 1959, **30**, 1259–1265.

5 C. Labanti, J. Wu, J. Shin, S. Limbu, S. Yun, F. Fang, S. Y. Park, C. Heo, Y. Lim, T. Choi, H.-J. Kim, H. Hong, B. Choi, K. Park, J. R. Durrant and J. Kim, *Nat. Commun.*, 2022, **13**, 3745.